Applied Surface Science 664 (2024) 160224

Contents lists available at ScienceDirect

Applied Surface Science

journal homepage: www.elsevier.com/locate/apsusc

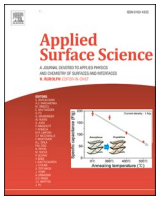

Full Length Article

Electro-assisted sorption behavior and mechanism of low-concentration rare earth elements on carbon based materials

Xuan Zhang [a,b], Weiquan Zhan [a,b,c,*], Qizheng Weng [a,b], Shaoxian Song [d], José Luis Arauz-Lara [c], Feifei Jia [a,b,**]

[a] Key Laboratory of Green Utilization of Critical Non-metallic Mineral Resources of Ministry of Education, Wuhan University of Technology, Wuhan 430070, Hubei, China
[b] School of Resources and Environmental Engineering, Wuhan University of Technology, Wuhan 430070, Hubei, China
[c] Instituto de Física, Universidad Autónoma de San Luis Potosí, Av. Manuel Nava 6, Zona Universitaria, San Luis Potosí 78290, México
[d] Instituto de Metalurgia, Universidad Autónoma de San Luis Potosí, Av. Sierra Leona 550, San Luis Potosí 78210, México

ARTICLE INFO

Keywords:
Electro-assisted sorption
Low-concentration
Rare earth elements
Carbon-based electrodes
Electric double layer capacitance

ABSTRACT

With increasing demands for rare earth elements (REEs) in high-tech and futuristic applications, developing efficient methods for recovering low-concentration REEs is necessary. Here, electro-assisted sorption of low-concentration REEs, La(III), Gd(III) and Y(III) (as symbol of light, medium, and heavy REEs) on carbon-based materials, activated carbon (AC), graphene, and graphite by a facile method was reported. Recovery of La (III), Gd(III) and Y(III) could reach ~100 % under low-concentration condition where the maximum adsorption capacity was up to 342.38 mg/(g·dm^2). Variants including applied voltage, electrodes-distance, pH, impurities, and concentration were considered to study the effects on REEs recovery. Interestingly, adsorption capacity and recovery under low voltage were respectively almost 20 and 14 folds than that without voltage, because voltage promoted REEs transfer and strengthened electrostatic interaction between electrodes and REEs. The mechanism for enhancing REEs recovery on carbon-based electrodes was resulted from high electric double layer (EDL) capacitance and low charge transfer resistance. Total desorption of REEs from electrodes could be quickly realized using NH_4Cl or HCl solution. Overall, the study gave a new insight of low-concentration REEs recovery using carbon-based materials, and provided an efficient route using electric method with porous materials for REEs recovery.

1. Introduction

Due to the special properties of rare earth elements (REEs), they play an important role in the transition toward green energy, for example, electric batteries [1,2], wind and solar energy [3,4], catalysis [5], semiconductors [6], luminescence [7]. The recovery of REEs from ores [8,9] and waste materials [10,11] was necessary for green development. Thus, many researches [12–17] have recently been proposed for developing techniques or materials for REEs recovery in aqueous solutions from low-grade resources, for instance, mining processing wastewater [18], refining wastewater [19], seawater [20], etc.

Various methods, such as, solvent extraction [21–23], ion exchange [24–26], chemical precipitation [27–30], and sorption [31–33] have been largely used in separating and recovering REEs. However, these approaches were hard for application due to large consumption of reagents, or high cost, or poor recovery [34]. In addition, most current methods focused on the recovery in high concentration [35–39], while rare researches were related with low concentration. There are still challenges to effectively recover REEs within low concentration range from aqueous solutions.

Electro-adsorption was a kind of promising way to adsorb low-concentration target ions in solution since the target ions were induced to overcome the electrostatic repulsion and towards the adsorbent under the electric field [40]. Materials as the working

* Corresponding author at: Key Laboratory of Green Utilization of Critical Non-metallic Mineral Resources of Ministry of Education, Wuhan University of Technology, Wuhan 430070, Hubei, China.
** Corresponding author at: Key Laboratory of Green Utilization of Critical Non-metallic Mineral Resources of Ministry of Education, Wuhan University of Technology, Wuhan 430070, Hubei, China.
E-mail addresses: zhan_weiquan@163.com (W. Zhan), feifeijia@whut.edu.cn (F. Jia).

https://doi.org/10.1016/j.apsusc.2024.160224
Received 3 March 2024; Received in revised form 24 April 2024; Accepted 4 May 2024
Available online 5 May 2024

electrodes are vital for the interaction between electrolyte and electrode [41]. The target ions are captured *via* physical interaction into the pores formed in EDL. According to the ion storage equation in EDL capacitance, $C = \frac{\varepsilon A}{d}$, capacitance is related with surface area [42]. As a result, porous electrode was beneficial for the recovery of low-concentration REEs.

Carbon materials, for instance, activated carbon (AC), graphite, graphene, carbon nanotubes, with their super porous structure, low cost, and high specific surface area properties have been found as common adsorbents for metal ions adsorption [43–45]. Few previous works [16,46] demonstrated that activated carbon electrode could bind with La(III), but focusing on the modification of AC and interaction with REEs. During the electro-adsorption process, the function of pores is indispensable. The adsorption process of REEs and role of pores on carbon electrode need to be further investigated. To our best knowledge, no studies extending electro-assisted sorption *via* carbon-based electrodes for low-concentration REEs recovery and related self-properties have been researched.

Herein, a facile device for electro-assisted sorption of low-concentration REEs from aqueous solutions using porous carbon materials was developed. AC, graphene, and graphite were selected as typical carbon materials. As for the representative light, middle and heavy REEs, La(III), Gd(III) and Y(III) were chosen for studying recovery, respectively. The aim is to provide the insights into recovering low-concentration REEs with porous carbon-based electrode in environmental application. The study was firstly carried out to deeply evaluate the recovery of low-concentration REEs in the EDL capacitance by porous structure of carbon-based electrodes.

2. Materials and methods

2.1. Materials

AC was provided as a commercial resource from the Sinopharm Chemical Reagent Company. Graphene is obtained from Xiamen Knano Graphene Technology Co., Ltd. Graphite powder was purchased from shanghai Macklin Biochemical Co., Ltd. Conductive carbon black was obtained from the Cabot Corporation. Lanthanum nitrate hexahydrate ($LaN_3O_9{\cdot}6H_2O$), gadolinium nitrate hexahydrate ($GdN_3O_9{\cdot}6H_2O$), yttrium nitrate hexahydrate ($YN_3O_9{\cdot}6H_2O$), and arsenazo III were purchased from Aladdin Co., China, while others (polytetrafluoroethylene ($(C_2F_4)n$), sodium hydroxide (NaOH), nitric acid (HNO_3), potassium chloride (KCl), sodium chloride (NaCl), magnesium chloride ($MgCl_2$), calcium chloride ($CaCl_2$), aluminum chloride hexahydrate ($AlCl_3{\cdot}6H_2O$), and iron chloride ($FeCl_3$)) were supplied by Sinopharm Chemical Reagent Company. The deionized water used in this work was produced by Millipore Milli-Q Direct 8/16 water purification system.

2.2. Fabrication of carbon-based electrodes

Carbon materials (AC, graphene, graphite), conductive carbon black, and polyvinylidene fluoride (dissolved in the DMA, 12.5 $mg{\cdot}mL^{-1}$), in an 8:1:1 mass ratio was mixed, and then the mixture was coated on titanium plate (Fig. S1). Afterwards, the electrodes were heated at 60 °C for 3 h to remove the residual organic solvent. The prepared electrodes were immerged in the deionized water for 24 h to keep shape. Finally, after drying in 60 °C for 1 h, the electrodes were used in the REEs recovery.

2.3. Electro-assisted REEs sorption

A self-made cell with an external power was applied for carrying out REEs recovery experiments (Fig. S2). The solution cycle was realized by a peristaltic pump at a rate of 45 rpm. At a certain time, 2.5 mL solution was extracted and filtered using 0.22 μm filter membrane. Following, the concentration of filtrate was detected by a UV–vis spectrophotometer (Lambda 750S). The adsorption capacity (Q) and recovery (R) were calculated by the following formula:

$$Q = (C_0 - C_t) \times \frac{(V_0 - V_t)}{A \bullet m} \quad (1)$$

$$R = (C_0 - C_t) \times \frac{1}{C_0} \quad (2)$$

where C_0 and C_t were the concentration of REEs at the initial and a certain moment, respectively, mg/L; V_0 and V_t meant the volume of reaction solution at the initial and a certain moment, respectively, L; A displayed the effective surface area of AC electrode, dm^2; m exhibited the mass used in the electrode, mg.

Variants including pH, voltage, initial concentration, and electrodes-distance were considered for investigating REEs recovery performances. REEs in the form of ions under pH of 1–6 was adjusted by HNO_3 and NaOH. Applied voltage was studied on the effect of REEs recovery in the range of 0 and 1.2 eV at pH of 5, concentration of 10 mg/L. Initial low concentration from 1 to 10 mg/L at pH of 5, applied voltage of 0.8 V was researched in REEs recovery. Effect of distance between electrodes including 3, 5, 7, and 9 mm on the REEs recovery was investigated.

2.4. Desorption and regeneration tests

After the recovery of REEs, the carbon-based electrode was immersed in a 100 mL solution of HCl (1 M) or NH_4Cl (1 M) without an external power to desorb REEs. 2 mL solution was extracted and filtered at a certain time. The desorption capacity and efficiency were calculated by the following formula:

$$D = C_d \times \frac{1}{C_0} \times 100\% \quad (3)$$

In which C_d was the concentration of REEs at a certain moment in the desorption experiment, mg/L.

2.5. Analyses

X-ray diffraction (XRD) with Cu-Kα radiation was applied on detecting the crystal structure of AC, D8 Advance, Bruker AXS, Germany. Transmission electron microscopy (TEM) was used to observe the morphology and microstructure of AC, JEM-F200 microscope, Japan. SEM was applied for investigating the morphologies of graphite and graphene, Phenom ProX G6, Netherlands. Raman was provided for studying the atomic bond structure of samples, INVIA Renishaw, England. X-ray photoelectron spectroscopy was performed on the analysis of elemental composition, Thermo Scientific K-alpha, America. Distribution of pore structure was studied by the specific surface and aperture analyzer, V-Sorb X800, China.

2.6. Electrochemical measurement

Electrochemical characteristic of titanium plate, AC, graphene, and graphic electrode including cyclic voltammetry (CV) and electrochemical impedance spectroscopy (EIS) was researched using VersaSTAT-450, PAR, America. A conventional three-electrode cell was applied on determining the electrochemical characteristics of titanium plate and AC electrode including cyclic voltammetry (CV) and electrochemical impedance spectroscopy (EIS) in a 1 M Na_2SO_4 solution. The three electrodes were platinum electrode (counter electrode), standard calomel electrode (reference electrode) and the titanium / AC electrode (working electrode).

2.7. REEs determination

The residual concentration of REEs in reaction solutions after adsorption on carbon-based electrodes was obtained by UV–vis spectrophotometer. Calibration curves were obtained as the following procedure. Firstly, a certain amount of REEs was dissolved in a 100 mL volumetric flask to obtain 2000 mg/L standard solution. After, various concentrations of REEs solution with 2 mL arsenazo III (0.5 g/L) was obtained in a 25 mL colorimetric tube. Here, arsenazo III acted as the role of chromogenic and complexing agent [47,48]. The absorbance of La(III), Gd(III) and Y(III) was measured at 655 nm, 651 nm, and 651 nm respectively. The calibration curves were obtained with the concentration of rare earth in the horizontal coordinate and the absorbance in the vertical coordinate, as shown in Fig. S3-5. All the correlation coefficient of R^2 were higher than 0.99, indicating that curve fitted well the relation between absorption and concentration. According to the fitting equation, the concentration of REEs was determined and calculated with three times to reduce the error.

3. Results and discussion

3.1. Characterization of carbon-based materials

Crystal structure of carbon materials, AC, graphite, and graphene was analyzed by XRD (Fig. 1a). The peak at around 25° in AC was detected, being caused by an almost amorphous structure in graphene [49]. As for graphite and graphene, typical characteristics of two sharp peaks located at about 26.5° and 54.5°, which derived from (0 0 2) and (0 0 4) planes of graphitic structure [50,51]. Chemical bond information in carbon materials was measured based on FTIR test, as shown in Fig. 1b. The adsorption peak at ~3440 cm^{-1} was due to the vibration (O–H) in hydroxyl groups [52]. Typical bands between 1700 and 1400 cm^{-1} were identified as characteristic of groups C=O stretching vibration in AC [53]. A situated band at 1152 cm^{-1} in AC was attributed to the C–O stretching vibration [54], and the radiation adsorption of the groups C–C=O in-plane bending vibration was present. Peaks at ~1096 and 1017 cm^{-1} demonstrated the presence of C-O functional groups [55]. In view of the provided XRD and FTIR results, the carbon materials were pure, while with hydroxyl groups.

The porous structure of carbon materials was evaluated from the adsorption–desorption isotherms of nitrogen by BET (Fig. 1c). When the relative pressure was during low value, the adsorption increased quickly, while there was hysteresis loop between 0.4 and 1.0 in the relative high pressure. The phenomenon demonstrated that coexistence of micropores and mesopores in carbon materials [56]. Enclosed area of AC was largest among the carbon materials, revealing that it had maximum pores content. For further investigating the pore structure of carbon materials, the mesoporous and macroporous pore size cumulation and distribution were exhibited in Fig. 1d and e, respectively. Regarding the mesopores, most pores distribution of carbon materials was located within 50 nm, which was beneficial for the formation of porous EDL and ions storage. As for microporous structure (Fig. 1f), the cumulative pore distribution sharply increased at the pore width between 0.75 and 1.00 nm and then slowly upper to 2.75 nm, demonstrating many micropores in AC, also the result could be directly seen through the distribution pore size (mainly located in the size range below 2 nm) [56]. All the specific surface area (SSA), volume, percentage of micro, meso and macropores for the carbon-based materials were summarized in Table S1. As seen in the contact angle results (Figure S6), the hydrophilic properties of the carbon materials were in the order of AC, graphene, and graphite, which was relevant with their SSA. The stronger hydrophilicity was due to higher SSA and more exposed oxygen-contained functional groups.

Morphologies and micro structures of carbon materials were characterized according to SEM and TEM. Graphite (Fig. 2a) showed a scale-like and flat surface, while graphene (Fig. 2b) displayed a rippled and crumpled structure, resulting in more reaction sites in graphene. According to the SEM image (Fig. 2c), AC exhibited rough morphology with highly interconnected pores (yellow dotted boxes). As shown in Fig. 2d, pores in AC could be clearly distinguished (green dotted boxes). The selected area electron diffraction (SAED) pattern in the inset picture suggested a certain crystallinity degree of AC, which was accordant with the consequence of XRD. Furthermore, the arranged lattice fringes with spacing of 0.349 nm (Fig. 2e) was originated from the (0 0 2) plane of graphite structure [57], which indicated the formation of graphite crystallites. Notably, a highly disordered structure (white dotted boxes)

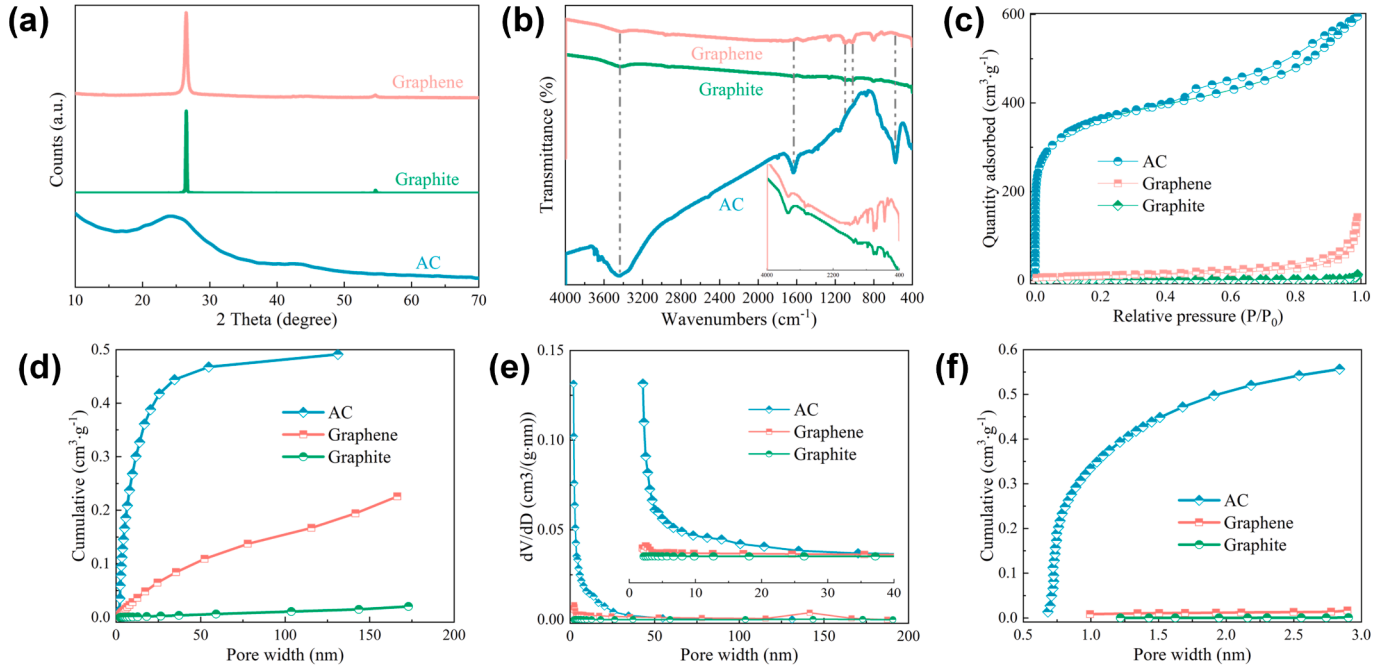

Fig. 1. (a) XRD patterns, (b) FTIR spectra, (c) nitrogen adsorption–desorption isotherms, (d) mesopores, macropores cumulation and (e) mesopores, macropores cumulation distribution, (f) micropores cumulation of carbon-based materials.

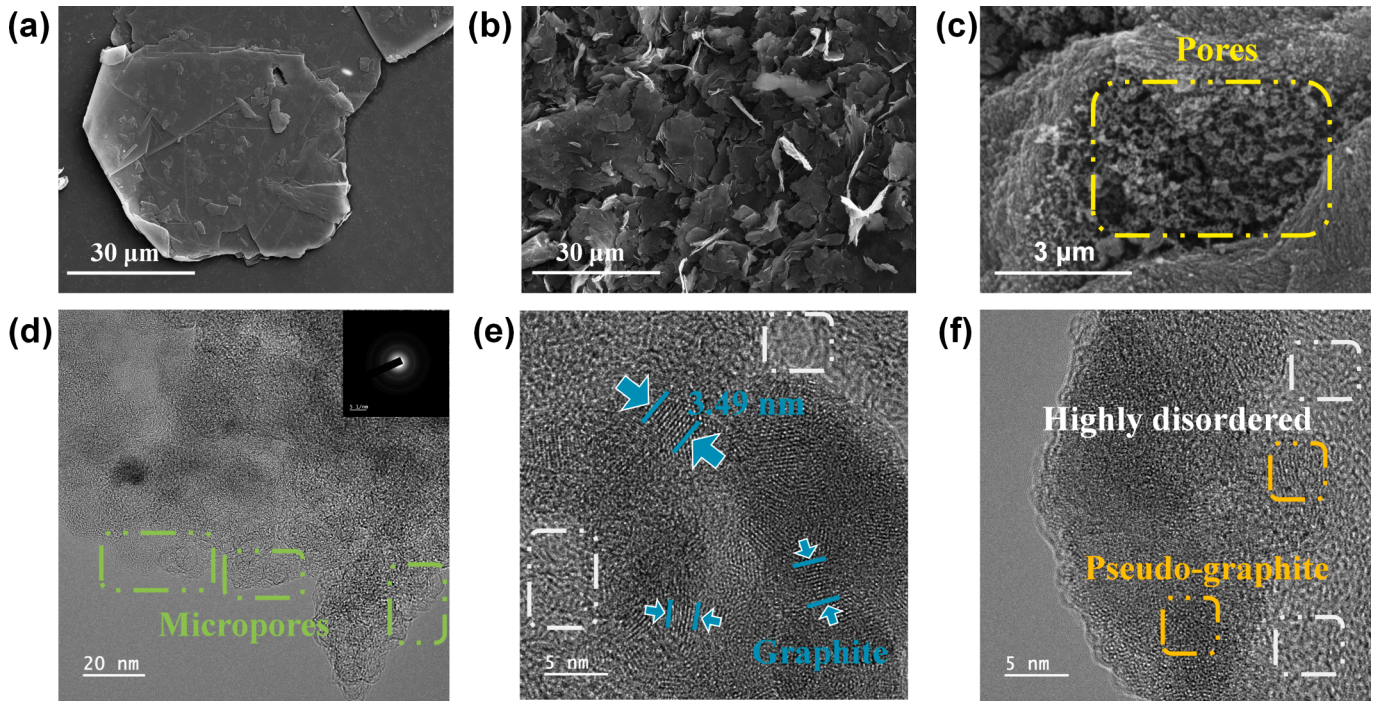

Fig. 2. SEM images of (a) graphite, (b) graphene and (c) AC. (d) TEM images and SAED pattern (as inset picture), (e, f) HRTEM images of AC.

with micropores and pseudo-graphic structures in the formation of graphite crystallite (orange dotted boxes) were proved in Fig. 2e and f [58]. Therefore, AC could be ascribed to porous graphitic carbon, and the abundant pores formed the EDL capacity for ion storage.

3.2. La(III) sorption performance evaluation

Electro-assisted La(III) sorption activity was performed on porous carbon materials, as shown in Fig. 3a and b. Adsorption capacity and related recovery of La(III) on carbon-based electrodes increased as time elapsed. Among all the carbon-based electrodes, AC electrode owned best La(III) recovery might originate from maximum pores content. Also, the recovery on graphene electrode was better than that on graphite electrode. As time passed, the La(III) adsorption on AC electrode tended to balance owing to the saturation of reaction sites, while growing tendency happened on graphene and graphite electrode because of more macropores for slow ions transfer. The maximum adsorption capacity according to simulation could achieve 342.38 mg/(g·dm^2), and

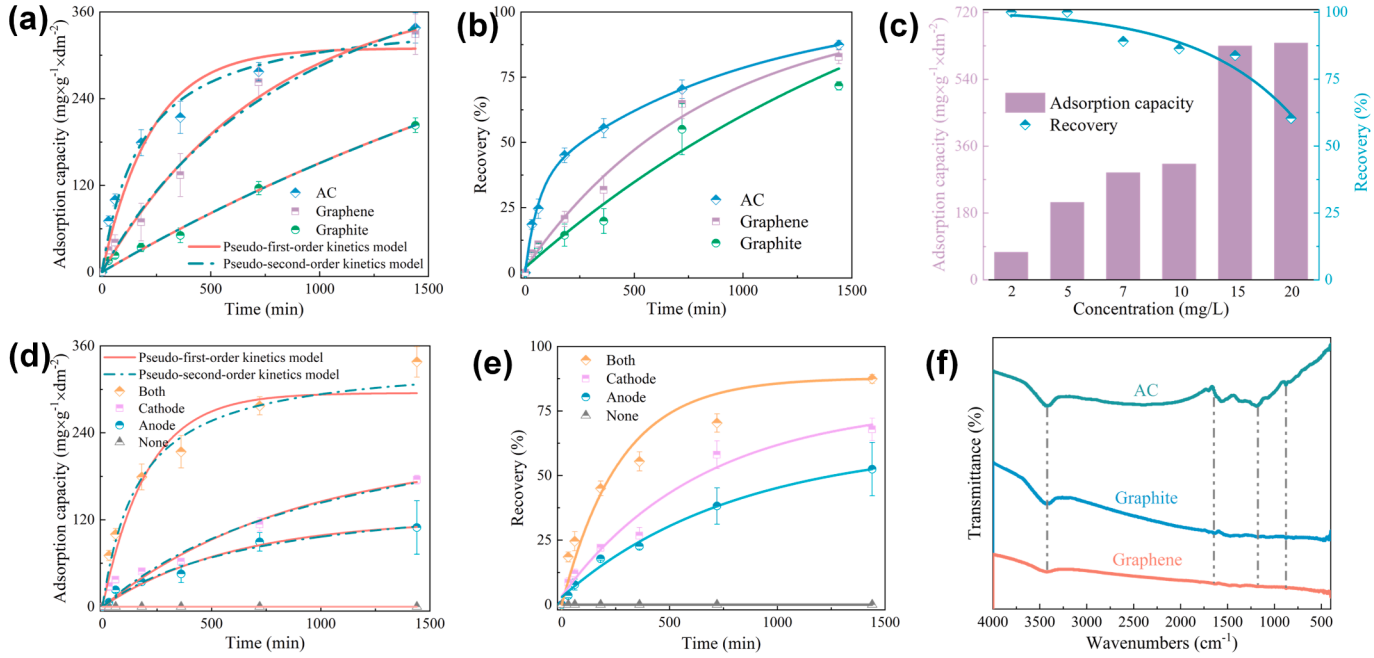

Fig. 3. REEs recovery performance by carbon-based electrode over time: (a) adsorption capacity and (b) recovery. (c) Recovery performance under various concentration by carbon-based electrode. (d) Adsorption capacity and (e) recovery on both and only one carbon-based electrode (cathode or anode), and without carbon-based electrode. (f) FTIR spectrum of carbon-based electrodes after La(III) recovery.

corresponding recovery was ~87 %. To compare with previous works, the adsorption capacity was adjusted to unified unit. From Table 1, the work showed great improvement in low-concentration REEs recovery. Apart from this, pseudo-first-order (Eq. (4)) and pseudo-second-order kinetic model (Eq. (5) [59,60] were applied for investigating the recovery process (Table 2).

$$q_t = q_e \times [1 - \exp(-k_1 t)] \quad (4)$$

$$q_t = \frac{t}{(t/q_e) + (1/k_2 q_e^2)} \quad (5)$$

where q_e and q_t were the adsorbed REEs at equilibrium time and t moment (min), respectively, mg/g; k_1 and k_2 were the first- and second-order rate constants, respectively, min^{-1}.

Adsorption process on AC electrode was more inclined to pseudo-second-order kinetic model, and it showed that chemical interaction might dominate during adsorption process. Regarding graphene and graphite electrode, the situation was highly consistent with two models, exhibiting the possible existence of physical and chemical interactions. The effect of initial concentration on the La(III) recovery using AC electrode was investigated (Fig. 3c). With increasing initial concentration, the adsorption capacity increased and then tended to balance due to the saturation of reaction sites. As a result, when the initial concentration was lower than 5 mg/L, the recovery reached ~100 %. Following, the recovery declined as the saturation of adsorption sites. Whatever, the CEC method by AC electrode obtained more than 85 % recovery as initial concentration bellowing 10 mg/L.

In Fig. 3d and e, adsorption capacity and corresponding recovery with both and only one AC electrode (cathode or anode), and without AC electrode were showed (Table 3). Adsorption capacity and recovery using both AC electrodes was higher than that by only one AC electrode, which could be ascribed to the rapid and mostly planar interelectrode diffusion within the trench, rapid diffusion of analyte into the trench, and improved specificity from two applied electrode potentials [61]. AC electrode as cathode reached better La(III) recovery performance than that as anode, because of the stronger electrostatic interaction in cathode. Without AC electrode, the adsorption capacity and recovery of La (III) via titanium plate was almost zero, indicating that there wasn't reaction between La(III) and titanium plate. When AC electrode was only used as cathode, the recovery was dominated by physical interaction, while contrast in the use of two AC electrodes, which demonstrated the existence of strong electrostatic interaction in cathode. To unravel the interaction between La(III) and reaction sites of carbon-based electrodes, FTIR was performed after the La(III) recovery, as shown in Fig. 3f. The peaks for stretching vibration of O–H, C=O and C–O shifted after the La(III) recovery compared with the result before adsorption [62], for instance, the C-O stretching vibration was 1152 cm^{-1} after adsorption, exhibiting the interaction between La(III) and oxygen-containing groups. Because of the existence of chemical interaction of La(III) and oxygen-containing groups, AC anode would adsorb a certain amount of La(III) as well when applying both AC electrodes for recovery.

Table 1
Comparison of La(III) adsorption capacity in the work with other literatures.

Adsorbents	Initial concentration (mg/L)	Adsorption capacity (mg/g)	Reference
Carbon nanotube	100	23.23	[63]
PA-MNPs	100	18.4	[64]
Activated carbon functionalized	50	10.14	[65]
Ca – Alginate Beads	25	6.373	[66]
Carboxylated cellulose filter	28	33.7	[67]
Ca – Alginate Beads	25	6.373	[66]
Fe_3O_4/GNPs	10	3.84	[68]
AC electrodes	9.84	61.63	This work

Table 2
Kinetic parameters for simulating La(III) recovery by carbon-based electrodes.

	Pseudo-first-order kinetic model		Pseudo-second-order kinetic model	
	q_e (mg/(g·dm^2))	R^2	q_e (mg/(g·dm^2))	R^2
AC	309.6591	0.9512	360.0251	0.9816
Graphene	393.8837	0.9872	585.0042	0.9847
Graphite	546.2353	0.9883	986.7876	0.9883

Table 3
Kinetic parameters for simulating recovery of La(III) on both and only one carbon-based electrode (cathode or anode), and without carbon-based electrode.

AC	Pseudo-first-order kinetic model		Pseudo-second-order kinetic model	
	q_e (mg/(g·dm^2))	R^2	q_e (mg/(g·dm^2))	R^2
Both	309.6591	0.9512	360.0251	0.9816
Cathode	213.8804	0.9435	222.1278	0.9475
Anode	120.7560	0.9751	166.1236	0.9753

3.3. La(III) sorption under experimental conditions

Environmental conditions including voltage, pH, distance between electrodes, and impurities were vital impact parameters for the REEs recovery. Applied voltage was an important key to influence La(III) recovery performance (Fig. 4a). Obviously, applied voltage enhanced adsorption capacity and recovery compared AC electrode without voltage. Adsorption capacity and recovery under 0.8 V were almost 20 and 14 folds than that without voltage, respectively. As the increase of applied voltage, the adsorption capacity and recovery enhanced quickly and then slowly, which was resulted from the saturation of electrostatic interaction sites on the surface of AC electrode. Furthermore, the effect of distance between two electrodes on recovery performances was considered (Fig. 4b). The far distance would decline La(III) recovery to some extent, being ascribed to the slow flux of solution between two electrodes. Solution pH was a factor that not only affecting the content of hydrogen ions but also the protonation of surface about AC electrode. With the increase of pH, the adsorption capacity and recovery were improved firstly and then reduced after pH of 5 (Fig. 4c). The enhanced recovery was due to strengthened electrostatic interaction that more negative charges on the surface of AC electrode (Fig. S7), while the declined recovery might be owing to the complex species of La(III). To evaluate the application of carbon-based electrode in actual treatment, AC electrode was used to test the selective recovery in a binary mixed solution (Fig. 4d). As observed, recovery was affected because of the competed adsorption by electrostatic interaction when the impurities were introduced. Cationic ions with a higher charge would be more easily absorbed onto the electrode. For ions with the same valence states, ions with a smaller hydrated radius are favorable for adsorption [69,70]. According this principle, Mg^{2+} influenced most among the impurities on the recovery, might be a reason of the small radius and high charges on competition for reactive sites.

3.4. Interaction between La(III) and carbon-based electrode

XPS was carried out for investigating the interaction role of oxygen species with REEs, a case of La(III), was carried out. From the survey spectra (Fig. 5a), the peaks for La appeared on both carbon-based cathode and carbon-based anode, indicating the adsorption of La(III). The existed interaction between La(III) and carbon-based materials and flu of solution led to the happen of adsorption on anode as well. High-resolution C 1*s* spectra (Fig. 5b) were deconvoluted into four parts, peaks at ~284.6, ~286.2, ~288.7, and ~291.0 eV caused by C=C, C–O, C=O and Π − Π* groups, respectively [58]. The shift of peaks in comparison of cathode and anode was resulted from the different loading dosage of La(III). For the high resolution La 3*d* spectra (Fig. 5c), there

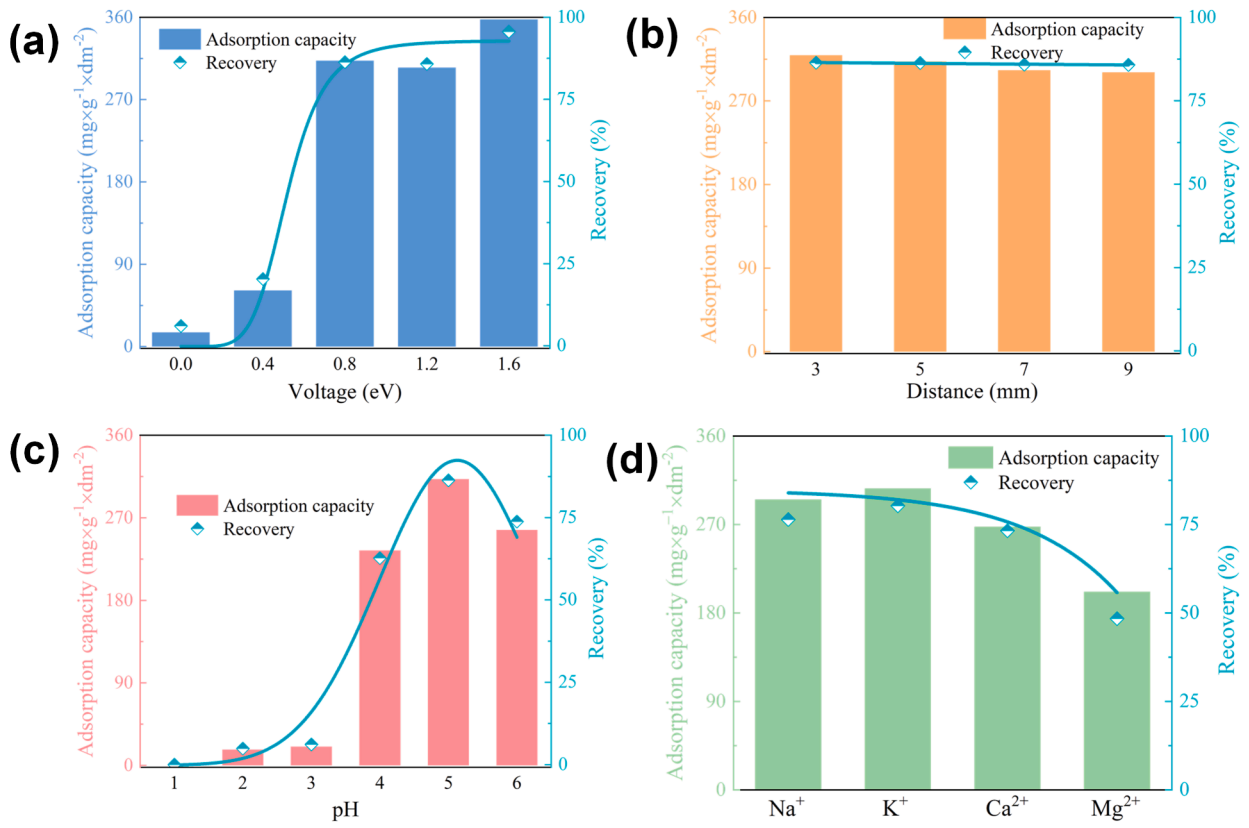

Fig. 4. Effect of La(III) recovery performance under different operative and environmental conditions: (a) applied voltage, (b) distance between two electrodes, (c) pH. (d) Selective recovery of La(III) in a binary mixed solution.

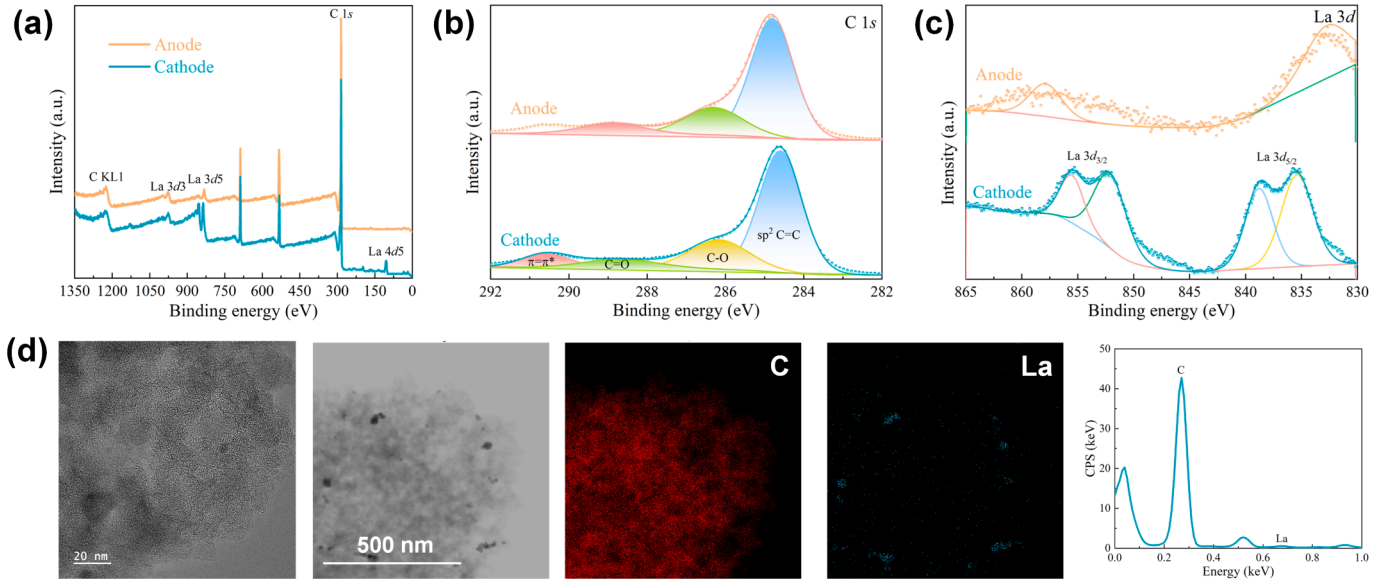

Fig. 5. (a) survey spectra, (b) high-resolution C 1*s* XPS spectra and (c) La 3*d* XPS spectra of AC electrode after La(III) recovery. (d) TEM images, EDS elemental distribution mapping: C and La, and EDS pattern of AC electrode after La(III) recovery.

are four fitted peaks at ~835.45, ~838.86, ~852.38 and ~855.58 eV, corresponding to the presence of La-N and La-O coordination bond [62]. Intensity of peaks in anode was weaker than that in cathode, showing that the La(III) adsorption mainly occurred in cathode. Besides, after the recovery, TEM images (Fig. 5d) displayed the similar morphology with that before adsorption, corresponding EDS elemental distribution and EDS pattern indicated the well-distribution of La(III) on the surface of electrode. On the basis of the above reported results, the recovery of La (III) on electrode *via* physical and chemical interaction was demonstrated.

3.5. *Extending recovery performances of Gd(III) and Y(III)*

To evaluate the actual application of REEs recovery, carbon-based

electrodes were applied in the recovery of medium and heavy REEs, Gd (III) and Y(III), in various concentrations. As shown in Fig. 6a and 6b, adsorption capacity and recovery of Gd(III) using AC electrode was highest among carbon-based electrodes, following as graphene electrode, graphite electrode. The difference might be owing to various electrochemical properties. AC electrode could reach ~100 % under initial concentration of 7 mg/L, and adsorption capacity was up to 305.87 mg/(g·dm^2). The higher concentration led to declined recovery due to saturated EDL capacity and active sites. According to SEM (Fig. 6c) and related EDS mapping (Fig. 6d) results, Gd(III) was recovered on carbon-based electrodes.

As for Y(III), sorption ability including adsorption capacity and recovery in Fig. 6e and 6f revealed the same tendency using carbon-based electrodes, in order of AC electrode, graphene electrode, and graphite electrode. Since similar physical and chemical properties of REEs, they behaved similar tendency on various carbon-based electrodes. Besides, recovery was 100 % using AC electrode when the initial concentration below 2 mg/L, with 100.32 mg/(g·dm^2). After recovery, carbon-based electrode was characterized by SEM-EDS, as shown in Fig. 6g and h. The results exhibited that the well-distributed and existence of Y elements. In all, comparing sorption ability of La(III), Gd(III), and Y(III) using carbon-based materials, AC electrode had best sorption ability, and then graphene electrode, graphite electrode, which was related with their different electrochemical behaviors. Referring to various REEs sorption on same carbon-based electrode, sorption capacity and recovery from high to low were La(III), Gd(III), and Y(III), which was owing to

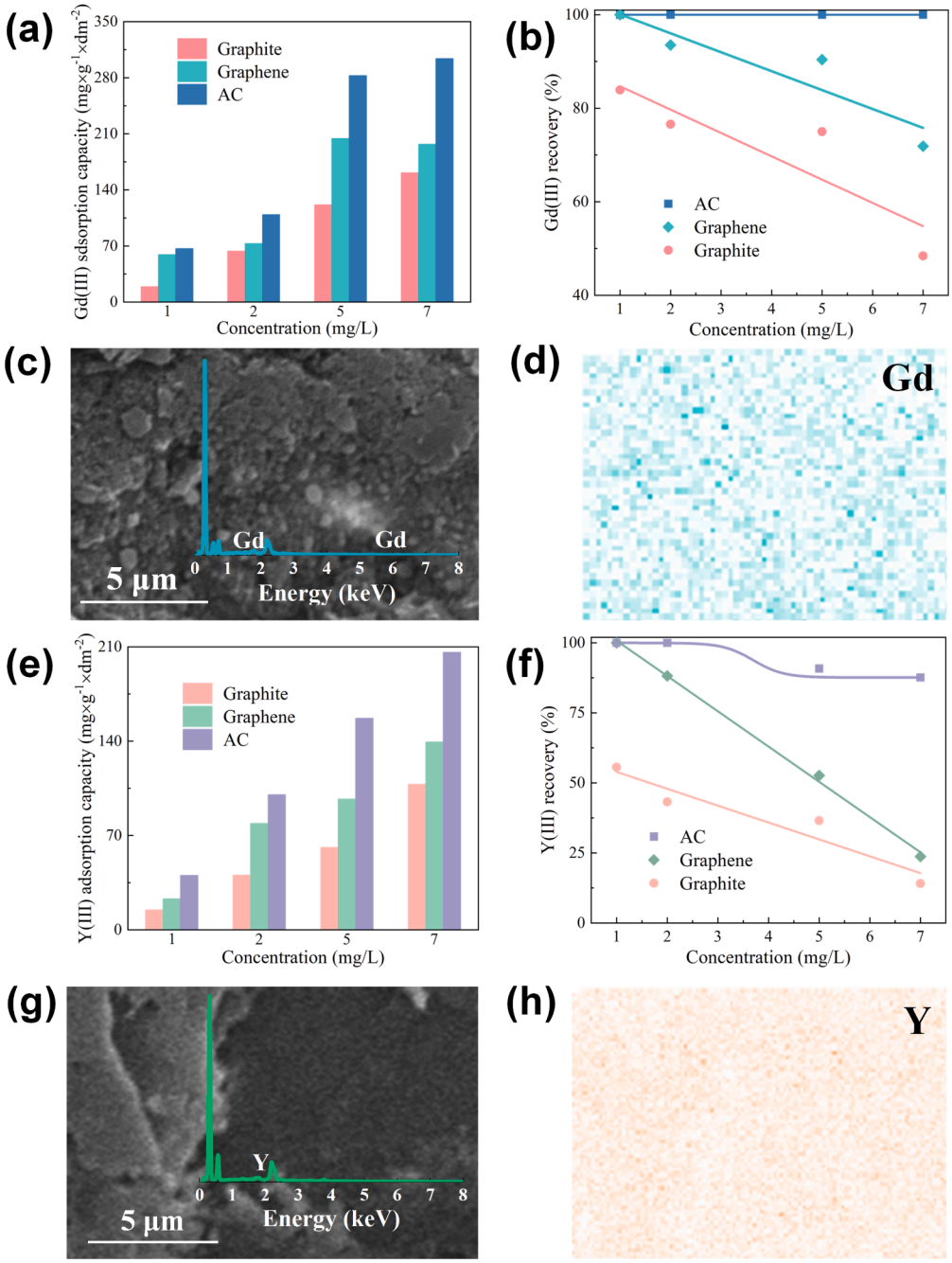

Fig. 6. (a) Adsorption capacity and (b) recovery of low-concentration Gd(III) on carbon-based electrodes. (c) SEM morphology and (d) corresponding EDS mapping of carbon-based electrode after Gd(III) sorption. (e) Adsorption capacity and (f) recovery of low-concentration Y(III) on carbon-based electrodes. (g) SEM morphology and (h) corresponding EDS mapping of carbon-based electrode after Y(III) sorption.

various configuration of extra-nuclear electron and solvent ion size.

3.6. Mechanism for REEs sorption on carbon-based electrodes

With the aim of revealing REEs storage ability in EDL, electrochemical measurements of carbon-based and titanium electrodes were conducted. CV curves at different scan rate for carbon-based electrodes were displayed in Fig. 7a, b and c. At low scan rate, the shape was rectangular, which demonstrated that there was enough time for ions to diffuse and enter the structure of carbon-based electrode. CV curves became leafy shape as the increase of scan rate due to the difficult diffusion of ions into the structure. At various scan rates, EDL capacity of carbon-based electrodes ranging from strong to weak was AC, graphene, and graphite, which was closely related to pores cumulation. Fig. 7d illustrated CV curves of carbon-based and titanium electrode in 1 M Na_2SO_4 solution at scan rate of 10 mV/s. AC electrode showed highest current intensity among all the electrodes, exhibiting the highest capacitance for REEs storage. As for titanium electrode, there is nearly no storage for REEs, which was correlated with recovery performance. As illustrated in Fig. 7e, sorption ability was no only related with storage, also the ion transfer originating from attraction. Ion diffusion was another non-negligible impactor in electro-assisted sorption process, and EIS was used to evaluate (Fig. 7f). The smaller diameter of semicircle meant the lower charge transfer resistance. AC electrode had relatively lowest resistance, resulting in a best electrochemical performance for the transfer of REEs. With more pores content, the transfer resistance was lower.

3.7. Desorption and characteristic of recycled electrode

Desorption studies were important for the reusability of electrode, as well as the recovery of targeted ions. Here, HCl and NH_4Cl were applied to investigate desorption ability of La(III) from carbon-based electrode. The desorption efficiency using HCl enhanced sharply and reached higher than 90 % within 20 min (Fig. 8a). As for desorption by NH_4Cl solution (Fig. 8c), the rate for desorption was slower than that using HCl, while the desorption reached almost 100 % within 120 min. In both ways for desorption, the desorbed La(III) concentration from cathode was higher than that from anode (also proved in the different color as insert picture of Fig. 8c, demonstrating that the La(III) adsorption mainly happened on cathode. The reusability of AC electrode by NH_4Cl (Fig. 8f) was stronger than that using HCl (Fig. 8d), because the instability of AC electrode in acid solution. After four circles, the adsorption capacity and recovery were still at a high level compared with the initial one when NH_4Cl was applied for reusing the AC electrode. In the desorption mechanism, REEs were desorbed by the monovalent ions and then transferred into solution as the form of soluble chlorides (Eqs. 6–7) [71,72].

$$C-O\cdots La^{3+}+HCl\rightarrow C-O\cdots H^{+}+LaCl_3 \quad (6)$$

$$C-O\cdots La^{3+}+NH_4Cl\rightarrow C-O\cdots NH_4{}^{+}+LaCl_3 \quad (7)$$

where *C* meant the carbon-based materials, *O* meant oxygen-contained groups including C–O and C=O.

The structure of AC after recycle was characterized by XRD and Raman tests. The crystal structure of graphite in AC was still existed (Fig. 8b). Meanwhile, two defined peaks at ~1326.67 and ~1588.04 cm^{-1} assigned to the D (sp3 defects) and G (sp2 hybridized carbons) was found [56], respectively (Fig. 8e), demonstrating the unchanged structure in AC. The above results presented a method for the regenerated application of CEC method by AC electrode.

4. Conclusions

Electro-assisted sorption of REEs by carbon-based materials has a great potential in low concentration range. All the carbon-based materials with porous structure showed efficient recovery of REEs. In the initial concentration of less than 5 mg/L, the recovery of La(III) was up to 100 %. The adsorption capacity of La(III) for AC electrode reached 368.20 mg/(g·dm^2). Gd(III) and Y(III) recovery using AC electrode obtained ~100 % under initial concentration of 7 and 2 mg/L, respectively, and the related adsorption capacity was 305.87 and 100.32 mg/(g·dm^2). The excellent recovery of REEs was resulted from high EDL capacity, strong electrostatic interaction from applied voltage and

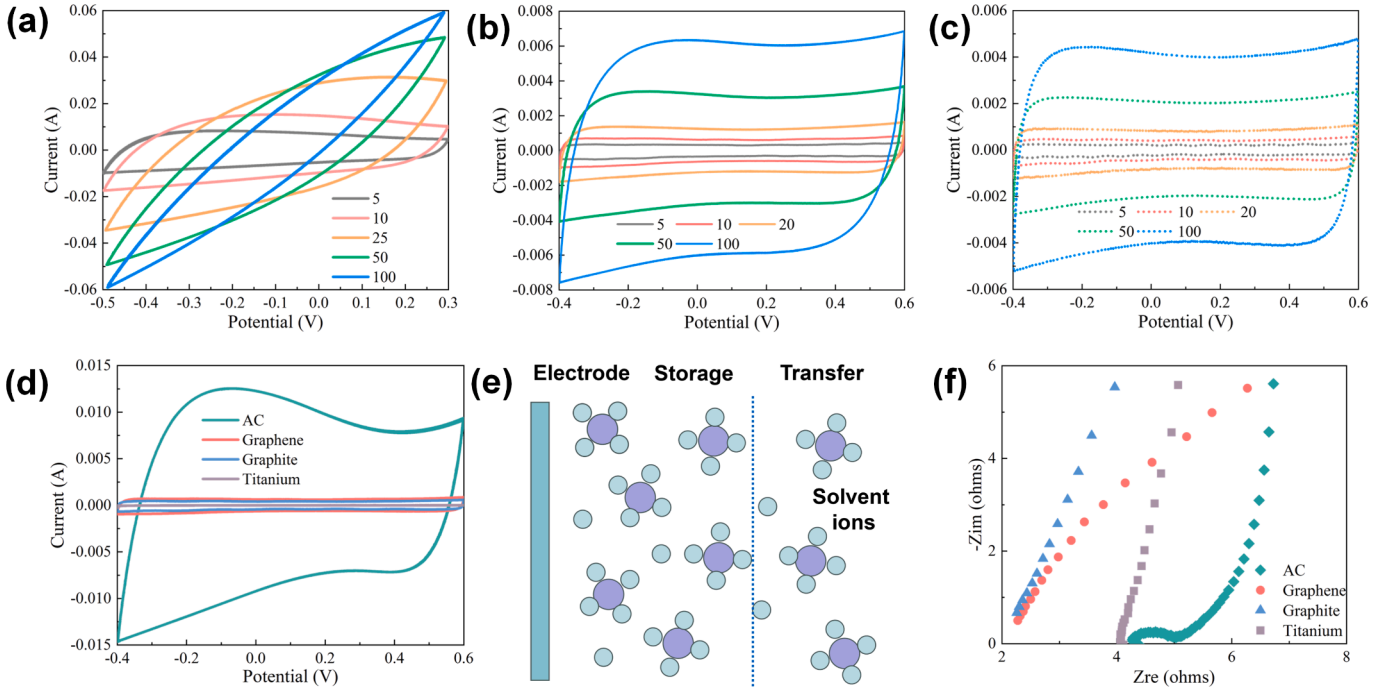

Fig. 7. Electrochemical performances: CV curves at different scan rate for (a) AC electrode, (b) graphene electrode and (c) graphite electrode. (e) Illustration for ions storage. (d) CV curves scanned at 10 mV/s and (f) EIS for carbon-based electrodes and titanium electrode.

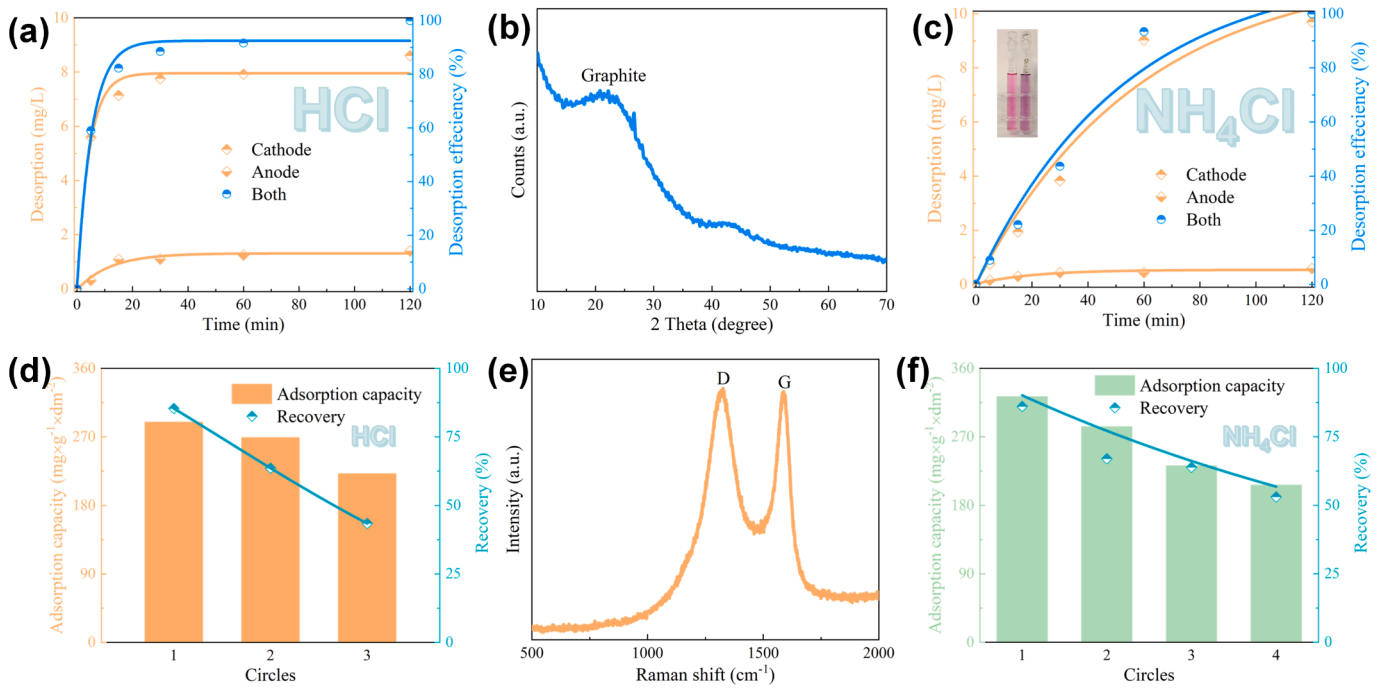

Fig. 8. The desorption efficiency of La(III) from AC electrode using (a) HCl and (c) NH_4Cl. The reusability of AC electrode by the desorption of (d) HCl and (f) NH_4Cl. (b) XRD pattern and (e) Raman spectrum of after recycle.

chemisorption from oxygen-containing groups. Higher applied voltage and lower distance between electrodes were beneficial for the recovery of REEs. Recovery performance was highly related with pores content and oxygen-containing group. More pores were better for REEs storage in EDL and transfer in aqueous solution. HCl and NH_4Cl were applied for desorbing REEs from carbon-based electrodes, respectively. High desorption efficiency (more than 90 %) within 20 min was obtained using HCl. Total desorption was realized by NH_4Cl solution, and the structure of carbon-based electrode was almost the same with before. After four cycles, the adsorption capacity and recovery declined owing to the dropped materials. The work provided a new insight for the recovery of low-concentration REEs from aqueous solutions based on carbon-based electrode.

CRediT authorship contribution statement

Xuan Zhang: Writing – original draft, Formal analysis, Methodology. **Weiquan Zhan:** Writing – review & editing, Supervision, Methodology. **Qizheng Weng:** Software, Investigation. **Shaoxian Song:** Data curation. **José Luis Arauz-Lara:** Conceptualization. **Feifei Jia:** Data curation, Supervision.

Declaration of competing interest

The authors declare that they have no known competing financial interests or personal relationships that could have appeared to influence the work reported in this paper.

Data availability

No data was used for the research described in the article.

Acknowledgements

The work is financially supported by the National Key Research and Development Program of China (2021YFC2900900), and the Natural Science Foundation of Hubei Province (ZRJQ2022000195). W. Zhan gratefully acknowledges the Consejo Nacional de Humanidades Ciencias y Tecnologías (CONAHCYT) of Mexico for offering him the scholarship under the grant No. 813934 during his Ph.D. studies.

Appendix A. Supplementary data

Supplementary data to this article can be found online at https://doi.org/10.1016/j.apsusc.2024.160224.

References

[1] H.S. Hirsh, Y. Li, D.H.S. Tan, M. Zhang, E. Zhao, Y.S. Meng, Sodium-ion batteries paving the way for grid energy storage, Adv. Energy Mater. 10 (2020) 2001274.
[2] P. Bombelli, A. Savanth, A. Scarampi, S.J.L. Rowden, D.H. Green, A. Erbe, E. Årstøl, I. Jevremovic, M.F. Hohmann-Marriott, S.P. Trasatti, E. Ozer, C.J. Howe, Powering a microprocessor by photosynthesis, Energy Environ Sci 15 (2022) 2529–2536.
[3] S. Ji, Y. Qu, T. Wang, Y. Chen, G. Wang, X. Li, J. Dong, Q. Chen, W. Zhang, Z. Zhang, S. Liang, R. Yu, Y. Wang, D. Wang, Y. Li, Rare-earth single erbium atoms for enhanced photocatalytic CO2 reduction, Angew. Chem. Int. Ed. 59 (2020) 10651–10657.
[4] B. Zheng, J. Fan, B. Chen, X. Qin, J. Wang, F. Wang, R. Deng, X. Liu, Rare-earth doping in nanostructured inorganic materials, Chem. Rev. 122 (2022) 5519–5603.
[5] R. Ryoo, J. Kim, C. Jo, S.W. Han, J.-C. Kim, H. Park, J. Han, H.S. Shin, J.W. Shin, Rare-earth–platinum alloy nanoparticles in mesoporous zeolite for catalysis, Nature 585 (2020) 221–224.
[6] J. Ran, G. Gao, F.-T. Li, T.-Y. Ma, A. Du, S.-Z. Qiao, Ti3C2 MXene co-catalyst on metal sulfide photo-absorbers for enhanced visible-light photocatalytic hydrogen production, Nat. Commun. 8 (2017) 13907.
[7] Y. Zhong, Z. Ma, S. Zhu, J. Yue, M. Zhang, A.L. Antaris, J. Yuan, R. Cui, H. Wan, Y. Zhou, W. Wang, N.F. Huang, J. Luo, Z. Hu, H. Dai, Boosting the down-shifting luminescence of rare-earth nanocrystals for biological imaging beyond 1500 nm, Nat. Commun. 8 (2017) 737.
[8] A.M. Borst, M.P. Smith, A.A. Finch, G. Estrade, C. Villanova-de-Benavent, P. Nason, E. Marquis, N.J. Horsburgh, K.M. Goodenough, C. Xu, J. Kynický, K. Geraki, Adsorption of rare earth elements in regolith-hosted clay deposits, Nat. Commun. 11 (2020) 4386.
[9] J. Pan, C. Zhou, M. Tang, S. Cao, C. Liu, N. Zhang, M. Wen, Y. Luo, T. Hu, W. Ji, Study on the modes of occurrence of rare earth elements in coal fly ash by statistics and a sequential chemical extraction procedure, Fuel 237 (2019) 555–565.
[10] T. Kegl, A. Kosak, A. Lobnik, Z. Novak, A.K. Kralj, I. Ban, Adsorption of rare earth metals from wastewater by nanomaterials: a review, J. Hazard Mater. 386 (2020).
[11] J. Lie, J.-C. Liu, Selective recovery of rare earth elements (REEs) from spent NiMH batteries by two-stage acid leaching, J. Environ. Chem. Eng. 9 (2021) 106084.
[12] D.L. Ramasamy, S. Porada, M. Sillanpää, Marine algae: a promising resource for the selective recovery of scandium and rare earth elements from aqueous systems, Chem. Eng. J. 371 (2019) 759–768.

[13] L. Omodara, S. Pitkäaho, E.-M. Turpeinen, P. Saavalainen, K. Oravisjärvi, R. L. Keiski, Recycling and substitution of light rare earth elements, cerium, lanthanum, neodymium, and praseodymium from end-of-life applications - a review, J. Clean Prod. 236 (2019) 117573.

[14] W. Zhang, R. Honaker, Characterization and recovery of rare earth elements and other critical metals (Co, Cr, Li, Mn, Sr, and V) from the calcination products of a coal refuse sample, Fuel 267 (2020) 117236.

[15] B. Li, Q. Kong, G. Wang, F. Liu, L. Guo, C. Liu, F. Liao, Z. Shi, Controls on the behaviors of rare earth elements in acidic and alkaline thermal springs, Appl. Geochem. 143 (2022) 105379.

[16] L. Wang, Y. Gao, Y. Chai, X. Sun, Recovery of rare earth by electro-sorption with sodium diphenylamine sulfonate modified activated carbon electrode, Sep. Purif. Technol. 292 (2022) 121005.

[17] W. Zhan, X. Zhang, Y. Yuan, Q. Weng, S. Song, M. de J. Martínez-López, J.L. Arauz-Lara, F. Jia, Regulating chemisorption and electrosorption activity for efficient uptake of rare earth elements in low concentration on oxygen-doped molybdenum disulfide, ACS Nano 18 (2024) 7298–7310.

[18] K. Pyrgaki, V. Gemeni, C. Karkalis, N. Koukouzas, P. Koutsovitis, P. Petrounias, Geochemical occurrence of rare earth elements in mining waste and mine water: a review, Minerals 11 (2021) 860.

[19] S. Costis, K.K. Mueller, L. Coudert, C.M. Neculita, N. Reynier, J.-F. Blais, Recovery potential of rare earth elements from mining and industrial residues: a review and cases studies, J. Geochem. Explor. 221 (2021) 106699.

[20] T. Sanada, N. Takamatsu, Y. Yoshiike, Geochemical interpretation of long-term variations in rare earth element concentrations in acidic hot spring waters from the Tamagawa geothermal area, Japan, Geothermics 35 (2006) 141–155.

[21] F. Xie, T.A. Zhang, D. Dreisinger, F. Doyle, A critical review on solvent extraction of rare earths from aqueous solutions, Miner. Eng. 56 (2014) 10–28.

[22] M. Zhang, X. Peng, J. Su, Z. Yang, S. Zeb, L. Li, C. Xu, Y. Zhao, G. Sun, Y. Cui, Highly efficient extraction separation of La3+ and Ce3+ with N, N, N′, N′-tetraisobutyl-3-oxadiglycolamide from mixed REEs, Sep. Purif. Technol. 258 (2021) 118012.

[23] R. Mu, J. Chen, D. Zou, K. Li, D. Li, Liquid-liquid extraction and recovery of Cerium (IV) and Phosphorus from sulfuric acid solution using Cyanex 923, Sep. Purif. Technol. 209 (2019) 351–358.

[24] Y. El Ouardi, S. Virolainen, E.S. Massima Mouele, M. Laatikainen, E. Repo, K. Laatikainen, The recent progress of ion exchange for the separation of rare earths from secondary resources – a review, Hydrometallurgy 218 (2023) 106047.

[25] Z. Chour, B. Laubie, J.L. Morel, Y. Tang, R. Qiu, M.-O. Simonnot, L. Muhr, Recovery of rare earth elements from Dicranopteris dichotoma by an enhanced ion exchange leaching process, Chem. Eng. Process. 130 (2018) 208–213.

[26] M. Hermassi, M. Granados, C. Valderrama, C. Ayora, J.L. Cortina, Recovery of rare earth elements from acidic mine waters: an unknown secondary resource, Sci. Total Environ. 810 (2022) 152258.

[27] Z. Liu, H. Zhou, W. Li, X. Luo, J. Wang, F. Liu, Separation and coextraction of REEs and Fe from NdFeB sludge by co-leaching and stepwise precipitation, Sep. Purif. Technol. 282 (2022) 119795.

[28] K. Binnemans, P.T. Jones, B. Blanpain, T. Van Gerven, Y. Yang, A. Walton, M. Buchert, Recycling of rare earths: a critical review, J. Clean. Prod. 51 (2013) 1–22.

[29] H.B. Trinh, J. Lee, S. Kim, J. Kim, Recovery of cerium from spent autocatalyst by sulfatizing–leaching–precipitation process, ACS Sustain. Chem. Eng. 8 (2020) 15630–15639.

[30] D. Li, Development course of separating rare earths with acid phosphorus extractants: a critical review, J. Rare Earth. 37 (2019) 468–486.

[31] S. Iftekhar, V. Srivastava, M. Sillanpää, Synthesis and application of LDH intercalated cellulose nanocomposite for separation of rare earth elements (REEs), Chem. Eng. J. 309 (2017) 130–139.

[32] X. Yang, D.K. Debeli, G. Shan, P. Pan, Selective adsorption and high recovery of La3+ using graphene oxide/poly (N-isopropyl acrylamide-maleic acid) cryogel, Chem. Eng. J. 379 (2020) 122335.

[33] T. Liu, J. Chen, Extraction and separation of heavy rare earth elements: a review, Sep. Purif. Technol. 276 (2021) 119263.

[34] M.F. Hamza, W.M. Abdellah, D.I. Zaki, Y.Z. Wei, K. Althumayri, W. Brostow, N. A. Hamad, A phosphonic functionalized biopolymer for the sorption of lanthanum (III) and application in the recovery of rare earth elements, Sustainability 15 (2023).

[35] R. Banda, H.S. Jeon, M.S. Lee, Solvent extraction separation of La from chloride solution containing Pr and Nd with Cyanex 272, Hydrometallurgy 121–124 (2012) 74–80.

[36] X. Su, Y. Wang, J. Su, W. Lai, Y. Gao, X. Sun, Enrichment of rare earths in magnesium sulfate leach solutions of ion-absorbed ores by extraction-precipitation, Hydrometallurgy 189 (2019) 105119.

[37] J. Su, X. Guo, Y. Gao, S. Wu, R. Xu, X. Sun, Recovery of thorium and rare earths from leachate of ion-absorbed rare earth radioactive residues with N1923 and Cyanex® 572, J. Rare Earth. 39 (2021) 1273–1281.

[38] P. Modi, A. Jamal, R. Varshney, I.C. Rahi, M.A. Siddiqui, Rare earth elements mobility, leaching and recovery by different chemicals treatment on coal samples and calcined samples of Sohagpur Coalfield, Madhya Pradesh, India, Int. J. Coal Prep. Util. 43 (2023) 148–168.

[39] A. Sachan, Enhanced Bioweathering of Coal for Rare Earth Element Extraction and Concentration, University of Alaska Fairbanks, 2019.

[40] M. Mao, T. Yan, J. Shen, J. Zhang, D. Zhang, Capacitive removal of heavy metal ions from wastewater *via* an electro-adsorption and electro-reaction coupling process, Environ. Sci. Technol. 55 (2021) 3333–3340.

[41] W. Zhan, Y. Yuan, X. Zhang, Y. Liang, S. Song, M. de Jesús Martínez-López, J.L. Arauz-Lara, F. Jia, Efficient and selective Lead(II) removal within a wide concentration range through chemisorption and electrosorption coupling process via defective MoS2 electrode, Sep. Purif. Technol. 329 (2024) 125183.

[42] Y. Liu, Y.-Y. Deng, Q. Zhang, H. Liu, Overview of recent developments of resource recovery from wastewater via electrochemistry-based technologies, Sci. Total Environ. 757 (2021) 143901.

[43] D. Campeau, D.F. León Rayo, A. Mansour, K. Muratov, F. Gagosz, Gold-catalyzed reactions of specially activated alkynes, allenes, and alkenes, Chem. Rev. 121 (2021) 8756–8867.

[44] K. Chaisiwamongkhol, C. Batchelor-McAuley, S.V. Sokolov, J. Holter, N.P. Young, R.G. Compton, Optimising carbon electrode materials for adsorptive stripping voltammetry, Appl. Mater. Today. 7 (2017) 60–66.

[45] Q. Weng, S. Song, W. Zhan, X. Zhang, Z. Xiang, J. Gao, F. Jia, Novel recovery of a low-concentration gold thiosulfate complex through electroreduction via a walnut shell charcoal electrode, Green and Smart, Min. Eng. 1 (2024) 58–66, https://doi.org/10.1016/j.gsme.2024.03.004.

[46] F. Zhao, S. Chen, H. Xiang, T. Gao, D. Wang, D. Wei, M. Sillanpää, Y. Ke, C.-J. Tang, Selectively capacitive recovery of rare earth elements from aqueous solution onto Lewis base sites of pyrrolic-N doped activated carbon electrodes, Carbon 197 (2022) 282–291.

[47] B. Zawisza, K. Pytlakowska, B. Feist, M. Polowniak, A. Kita, R. Sitko, Determination of rare earth elements by spectroscopic techniques: a review, J. Anal. At. Spectrom. 26 (2011) 2373.

[48] J.S. Fritz, M.J. Richard, W.J. Lane, Spectrophotometric determination of rare earths, Anal. Chem. 30 (1958) 1776–1779, https://doi.org/10.1021/ac60143a016.

[49] E.M. Iannicelli-Zubiani, P. Gallo Stampino, C. Cristiani, G. Dotelli, Enhanced lanthanum adsorption by amine modified activated carbon, Chem. Eng. J. 341 (2018) 75–82.

[50] D. Liu, Z. Yang, W. Li, S. Qiu, Y. Luo, Electrochemical intercalation of potassium into graphite in KF melt, Electrochim. Acta 55 (2010) 1013–1018.

[51] J. Guo, Z. Chen, Z.M. El-Bahy, H. Liu, H.M. Abo-Dief, W. Abdul, K.M. Abualnaja, A. K. Alanazi, P. Zhang, M. Huang, G. Hu, J. Zhu, Tunable negative dielectric properties of magnetic CoFe2O4/graphite-polypyrrole metacomposites, Adv. Compos. Hybrid Mater. 5 (2022) 899–906.

[52] A. Macías-García, M. Gómez Corzo, M. Alfaro Domínguez, M. Alexandre Franco, J. Martínez Naharro, Study of the adsorption and electroadsorption process of Cu (II) ions within thermally and chemically modified activated carbon, J. Hazard Mater. 328 (2017) 46–55.

[53] M.J. Bleda-Martínez, J.A. Maciá-Agulló, D. Lozano-Castelló, E. Morallón, D. Cazorla-Amorós, A. Linares-Solano, Role of surface chemistry on electric double layer capacitance of carbon materials, Carbon 43 (2005) 2677–2684.

[54] Q. Chen, Study on the adsorption of lanthanum(III) from aqueous solution by bamboo charcoal, J. Rare Earth. 28 (2010) 125–131.

[55] A.D. Pingale, A. Owhal, A.S. Katarkar, S.U. Belgamwar, J.S. Rathore, Facile synthesis of graphene by ultrasonic-assisted electrochemical exfoliation of graphite, Mater. Today Proc. 44 (2021) 467–472.

[56] Y. Yao, G. Huang, Y. Liu, Y. Liu, Y. Li, G. Han, B. Xing, Q. Liu, J. Jia, C. Zhang, Facile synthesis of B/N co-doped porous carbon nanosheets with high heteroatom content and electrical conductivity for excellent-performance supercapacitors, Appl. Surf. Sci. 580 (2022) 152236.

[57] Y. Yao, G. Huang, Y. Liu, Y. Li, G. Han, W. Kang, B. Xing, Q. Liu, J. Jia, C. Zhang, Microstructure modification of porous carbon induced by low-dosage manganese nitrate for high-performance supercapacitor electrode, Electrochim. Acta 408 (2022) 139928.

[58] Y. Liu, G. Huang, Y. Li, Y. Yao, Q. Liu, B. Xing, J. Jia, C. Zhang, Structural evolution of porous graphitic carbon nanosheets based on quinonyl decomposition for supercapacitor electrodes, Appl. Surf. Sci. 537 (2021) 147824.

[59] W. Zhan, F. Jia, Y. Yuan, C. Liu, K. Sun, B. Yang, S. Song, Controllable incorporation of oxygen in MoS2 for efficient adsorption of Hg2+ in aqueous solutions, J. Hazard Mater. 384 (2020) 121382.

[60] F. Jia, Q. Wang, J. Wu, Y. Li, S. Song, Two-dimensional molybdenum disulfide as a superb adsorbent for removing Hg2+ from water, ACS Sust. Chem. Eng. 5 (2017) 7410–7419.

[61] J.L. Hammond, A.J. Gross, P. Estrela, J. Iniesta, S.J. Green, C.P. Winlove, P. G. Winyard, N. Benjamin, F. Marken, Cysteine-cystine redox cycling in a gold-gold dual-plate generator-collector microtrench sensor, Anal. Chem. 86 (2014) 6748–6752.

[62] F. Zhao, E. Repo, Y. Song, D. Yin, S. Ben Hammouda, L. Chen, S. Kalliola, J. Tang, K.C. Tam, M. Sillanpää, Polyethylenimine-cross-linked cellulose nanocrystals for highly efficient recovery of rare earth elements from water and a mechanism study, Green Chem. 19 (2017) 4816–4828.

[63] L. Huang, L. Liu, W. Huang, B. Zhao, Z. Shen, Y. Bao, H. Znad, Recovery of lanthanum cations by functionalized magnetic multi-walled carbon nanotube bundles, RSC Adv. 11 (2021) 4751–4759.

[64] J. Gaete, L. Molina, F. Valenzuela, C. Basualto, Recovery of lanthanum, praseodymium and samarium by adsorption using magnetic nanoparticles functionalized with a phosphonic group, Hydrometallurgy 203 (2021) 105698.

[65] N.S. Awwad, H.M.H. Gad, M.I. Ahmad, H.F. Aly, Sorption of lanthanum and erbium from aqueous solution by activated carbon prepared from rice husk, Colloids Surf. B 81 (2010) 593–599.

[66] D. Song, S.-J. Park, H.W. Kang, S. Bin Park, J.-I. Han, Recovery of lithium(I), Strontium(II), and lanthanum(III) using Ca–Alginate beads, J. Chem. Eng. Data 58 (2013) 2455–2464.

[67] C. Li, H. Ma, S. Venkateswaran, B.S. Hsiao, Sustainable carboxylated cellulose filters for efficient removal and recovery of lanthanum, Environ. Res. 188 (2020) 109685.
[68] E.L. Afonso, L. Carvalho, S. Fateixa, C.O. Amorim, V.S. Amaral, C. Vale, E. Pereira, C.M. Silva, T. Trindade, C.B. Lopes, Can contaminated waters or wastewater be alternative sources for technology-critical elements? The case of removal and recovery of lanthanides, J. Hazard. Mater. 380 (2019) 120845.
[69] X. Liu, J. Wu, J. Wang, Electro-enhanced removal of cobalt ions from aqueous solution by capacitive deionization, Sci. Total Environ. 697 (2019) 134144.
[70] R. Chen, T. Sheehan, J.L. Ng, M. Brucks, X. Su, Capacitive deionization and electrosorption for heavy metal removal, Environ. Sci. 6 (2020) 258–282.
[71] G.A. Moldoveanu, V.G. Papangelakis, Recovery of rare earth elements adsorbed on clay minerals: I. Desorption mechanism, Hydrometallurgy 117–118 (2012) 71–78.
[72] M.T. Ochsenkühn-Petropoulou, K.S. Hatzilyberis, L.N. Mendrinos, C.E. Salmas, Pilot-plant investigation of the leaching process for the recovery of scandium from red mud, Ind. Eng. Chem. Res. 41 (2002) 5794–5801.